Acta Oceanol. Sin., 2017, Vol. 36, No. 5, P. 26–30
DOI: 10.1007/s13131-017-1067-2
http://www.hyxb.org.cn
E-mail: hyxbe@263.net

The variation of turbulent diapycnal mixing at 18°N in the South China Sea stirred by wind stress

LIU Yongzheng[1, 2*], JING Zhao[1, 2, 3], WU Lixin[1, 2]

[1] Physical Oceanography Laboratory, Ocean University of China/CIMST, Qingdao 266100, China

[2] Qingdao National Laboratory for Marine Science and Technology, Qingdao 266100, China

[3] Department of Oceanography, Texas A&M University, College Station, TX 77843-3146, USA

Received 19 March 2016; accepted 1 September 2016

Abstract

The spatial and temporal variations of turbulent diapycnal mixing along 18°N in the South China Sea (SCS) are estimated by a fine-scale parameterization method based on strain, which is obtained from CTD measurements in yearly September from 2004 to 2010. The section mean diffusivity can reach ~10^{-4} m^2/s, which is an order of magnitude larger than the value in the open ocean. Both internal tides and wind-generated near-inertial internal waves play an important role in furnishing the diapycnal mixing here. The former dominates the diapycnal mixing in the deep ocean and makes nonnegligible contribution in the upper ocean, leading to enhanced diapycnal mixing throughout the water column over rough topography. In contrast, the influence of the wind-induced near-inertial internal wave is mainly confined to the upper ocean. Over both flat and rough bathymetries, the diapycnal diffusivity has a growth trend from 2005 to 2010 in the upper 700 m, which results from the increase of wind work on the near-inertial motions.

Key words: diapycnal mixing, diffusivity, wind-induced near-inertial internal wave, topography

Citation: Liu Yongzheng, Jing Zhao, Wu Lixin. 2017. The variation of turbulent diapycnal mixing at 18°N in the South China Sea stirred by wind stress. Acta Oceanologica Sinica, 36(5): 26–30, doi: 10.1007/s13131-017-1067-2

1 Introduction

Diapycnal mixing plays an important role in modifying water mass, transporting heat and maintaining ocean stratification. Understanding its spatial and temporal variations is key to the improvement of numerical model representation of large-scale ocean circulation and climate changes. Away from boundaries, diapycnal mixing occurs mainly through internal wave breaking. Winds and tides input a primary energy into the internal wave field (Wunsch and Ferrari, 2004). The heterogeneity of the energy sources leads to pronounced spatial variability of diapycnal mixing, which has been clearly revealed by measurements in the past three decades (e.g., Gregg, 1987; Kunze et al., 2006; Wu et al., 2011; Whalen et al., 2012; Waterhouse et al., 2014). An enhanced diapycnal diffusivity is found over the rough topography due to interactions of the bottom geostrophic or tidal flow with topography and under the storm tracks due to an energetic near-inertial energy flux into the ocean.

Strong internal tides are generated over the rough topography around the Luzon Strait and propagate westwards into the South China Sea (SCS) (Alford et al., 2015). Previous measurements along 21°N (Tian et al., 2009) revealed the enhanced diapycnal mixing in the deep ocean of the SCS and attributed it to the dissipation of energetic internal tides generated around the Luzon Strait. However, it remains unclear what are the energy sources responsible for the diapycnal mixing in the region of the SCS to the south of the Luzon Strait where the internal energy flux is much weaker (Alford et al., 2015). In particular, the wind-generated near-inertial internal waves may play a significant role in furnishing diapycnal mixing there, which remains poorly assessed.

In this paper, we analyze the variation of turbulent diapycnal mixing to the south of Luzon Strait and its controlling factors based on the CTD profiles collected along 18°N by the Key Laboratory of Tropical Marine Environment Dynamics, the South China Institute of Oceanology, the Chinese Academy of Sciences. The diapycnal diffusivity is inferred from a fine-scale parameterization following Kunze et al. (2006). The paper is organized as follows. Methodology and data are introduced in Section 2. Results and analysis are shown on Section 3. Finally, summary and some discussion are given in Section 4.

2 Methodology and data

2.1 *Fine-scale parameterization method*

The diapycnal diffusivity (Kunze et al., 2006; Polzin et al., 1995; Gregg et al., 2003) can be calculated in terms of a fine-scale strain as

$$K = K_0 \frac{\langle \xi_z^2 \rangle^2}{\mathrm{GM}\,\langle \xi_z^2 \rangle^2} h_2(R_\omega) j(f/N), \quad (1)$$

Foundation item: The National Basic Research Program (973 Program) of China under contract No. 2013CB956201; the National Natural Science Foundation of China under contract Nos 41521091, U1406401 and 41622602; the Global Change Project under contract No. GASI-03-01-01-05.

*Corresponding author, E-mail: lyzh6699@163.com

$$h_2(R_\omega) = \frac{1}{6\sqrt{2}} \frac{R_\omega(R_\omega+1)}{\sqrt{R_\omega-1}}, \tag{2}$$

$$j(f/N) = \frac{f\cosh^{-1}(N/f)}{f_{30}\cosh^{-1}(N_0/f_{30})}, \tag{3}$$

where K_0=0.05×10^{-4} m^2/s, $\langle \xi_z^2 \rangle$ represents the strain variances, $_{GM}\langle \xi_z^2 \rangle$ is the strain variances from the GM model spectrum (Gregg and Kunze, 1991; K unze et al., 1992), R_ω is the shear/strain ratio, f is the Coriolis parameter, N is buoyancy frequency, $f_{30} = f(30°\mathrm{N})$, and N_0=5.2×10^{-3} rad/s. The other details followed Kunze et al. (2006).

Given the fact that the strain spectrum can be contaminated by CTD noise and background stratification, we cannot apply the methodology to the regions that display shape pycnoclines and weak stratification. In this paper, the ratio of the shear to the strain is set to be an constant number of 7 proposed by Kunze et al. (2006), for the reason that profiles of horizontal velocity are not available.

2.2 *The roles of near-inertial winds*

The flux from wind to inertial motions can be computed from a local slab mixed-layer model (Pollard and Millard, 1970):

$$\frac{\mathrm{d}z}{\mathrm{d}t} + (r + \mathrm{i}f)z = \frac{T}{H}, \tag{4}$$

where $z = u + \mathrm{i}v$, is the mixed-layer current; $T = \rho^{-1}(\tau_x + \mathrm{i}\tau_y)$, represents the wind stress; ρ is the density of seawater (1 025 kg/m^3); H is the mixed-layer depth (MLD), which equals 50 m (Alford, 2001); and r is a frequency-dependent damping coefficient (Alford, 2003):

$$r = r_0(1 - \mathrm{e}^{-\sigma^2/2\sigma_c^2}), \tag{5}$$

where σ represents the angular frequency which related to $T(\sigma)$, $T(\sigma)$ is obtained from Fourier transforming the wind-stress time series, r_0=0.15 f, and σ_c=f/2.

Time-domain solutions to Eq. (4) are impossible, but the solution via a spectrum can be computed (Alford, 2003), for the transfer function, $R \equiv Z(\sigma)/T(\sigma)$, to Eq. (4) is

$$R(\sigma) = \frac{1}{H} \frac{r - \mathrm{i}(f+\sigma)}{r^2 + (f+\sigma)^2}. \tag{6}$$

In this work, the expression for the flux is $\Pi(H) = \mathrm{Re}[\rho Z T^*]$ based on the results by Alford (2003). The other details are followed by Alford (2003).

2.3 *Data*

The CTD profiles (Fig. 1) at 18°N, which covered 110°–120°E, had a time span from 2004 to 2010 in every September in the SCS region, provided from the Key Laboratory of Tropical Marine Environment Dynamics, the South China Sea Institute of Oceanology the Chinese Academy of Sciences. The accuracies of conductivity, temperature and pressure were 0.000 3 S/m, 0.001°C and 0.015%, respectively. Only profiles with the vertical resolution within 1 m were used. The downward data from CTD were used. All the profiles were divided into 256 m long segments, and the segment of 0–256 m was discarded given that the presence of sharp pycnoclines. A linear fit was removed and the segments were windowed at both ends with 10% sin^2 tapers before Fourier transforming (Kunze et al., 2006).

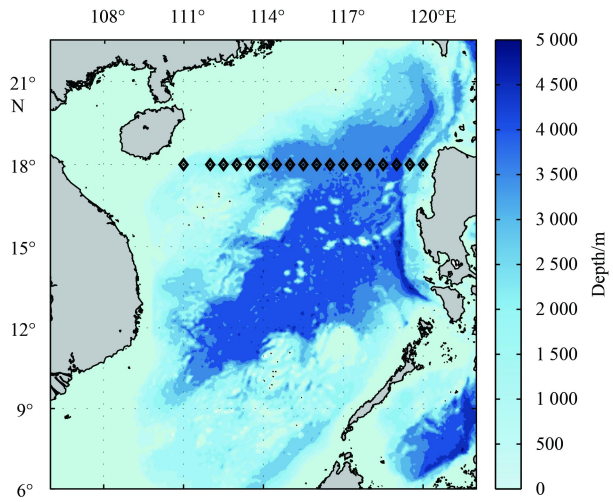

Fig. 1. Location of the CTD profiles (black diamond). Color map in blue shows the topography of the South China Sea from ETOPO1 (ice). Subjecting to typhoon or other limitations, each walking observation could not cover all stations. For some of detailed descriptions referred to Ge et al. (2012).

The NCAR/NCEP reanalysis 4-times daily wind-speed data at 10 m which were calculated for wind stress spanning from the year 2004 to the year 2010 were used in this work. At each grid, interpolating time series of each year onto 8 min grid (Alford, 2003). Finally, the wind flux was daily averaged to match the *in situ* observations.

The data from Grid of Earth's surface depicting the top of the Antarctic and Greenland ice sheets (1 min resolution) were used for computing topographic roughness (Jayne and St Laurent, 2001).

3 Results and analysis

We first evaluated the time-mean diapycnal diffusivity K based on the CTD profiles via fine-scale parameterization method. There were two identified features. First, the diffusivity near the bottom is redder than that in upper column. In some longitude, the diffusivity near the bottom, which could reach 10^{-2} m^2/s, is two or three order of magnitude stronger than that in the upper column (e.g., around 18°N, 113°E, 119°E and 119.5°E, see Fig. 2). The diffusivity averaged over all segments could reach the magnitude of 10^{-4} m^2/s in the SCS (Fig. 3), which was enhanced compared with that in the open ocean (Kunze et al., 2006). In the upper ocean, the vertical averaged (first four segments) diffusivity was an order magnitude less than the full depth averaged diffusivity. A temporal-vertical averaged (all segments) diffusivity is various with the topography (Fig. 3). It is found that the diffusivity can exceed to 10^{-4} m^2/s and even reached 10^{-2} m^2/s near the rough topography (Fig. 3), which is probably due to the dissipation of internal tides from barotropic flow (Egbert and Ray, 2001; Wunsch and Ferrari, 2004; Tian et al., 2009). Second, over flat abyssal basins, where the internal energy flux is much weaker, the mean diffusivity of upper four segments can over 4.5×10^{-5} m^2/s (Fig. 2), which is stronger than that in the outside Pacific (10^{-6}–10^{-5} m^2/s).

In order to focus on the variation of diapycnal turbulence diffusivity, the regional averaged diffusivity based on the roughness

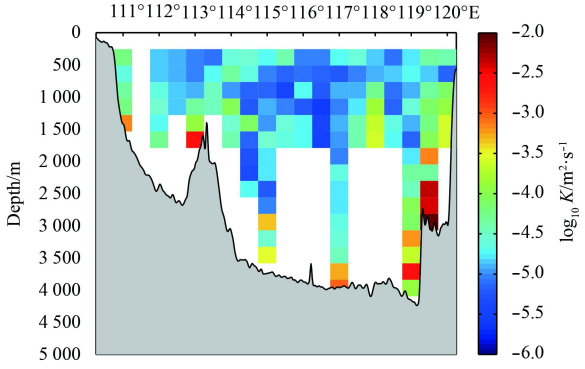

Fig. 2. Depth-longitude distribution of the time-mean turbulent diffusivity based on a fine-scale parameterization method.

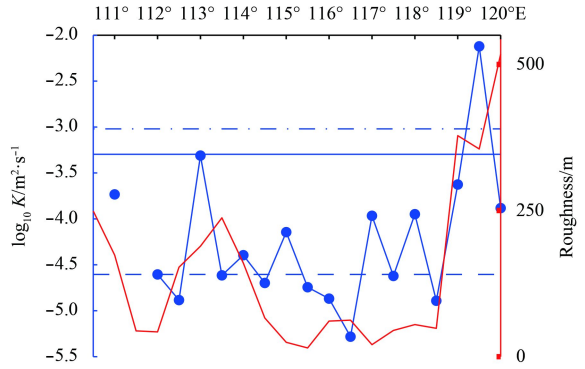

Fig. 3. Vertically averaged diffusivity against longitude (blue thick solid) as well as the mean-square bottom roughness following Jayne and St Laurent (2001) (red thick solid). The blue thin solid line represents the zonal mean of the vertically averaged diffusivity. The blue dashed line represents the zonal mean of the averaged diffusivity upper 1 000 m. The blue dash-dot line represents the zonal mean of the averaged diffusivity below 1 000 m.

of each segment in the upper ocean was analyzed respectively (Figs 4 and 5). We selected 114.5°–118.5°E as smooth region and 119°–120°E as rough region (Fig. 3). For the flat region, we sieved data from 2006 to 2010. While in the rough region, only the year of 2005, 2006, 2007 and 2010 could be selected. Missing year due to the lack of data in the selected area. All of the three segments (256–512, 513–768 and 769 –1 024) in the flat region had an increasing trend, even though it varied in each year (Fig. 4). The features in the rough region were more remarkable. All of four upper segments shown an increasing trend in the first 3 a despite the diffusivity of all four segments slight decrease in 2010. It could be identified that the turbulent diapycnal diffusivity has enhanced from 2005 to 2010 in this area (Fig. 5). So both regions had increased in the diapycnal diffusivity in the upper ocean from 2006 to 2010.

Wind-work input great amount of energy on ocean inertial motions (Gill et al., 1974; Alford, 2001), which can affect local diapycnal mixing (Jing et al., 2011; Jing and Wu, 2014; Li and Xu, 2014). Jing and Wu (2010) had found a significant correlation between the diapycnal diffusivity and the wind stress, meanwhile wind-induced downward-propagating near-inertial wave can input the energy for mixing (Jing et al., 2011; Jing and Wu, 2014; Li and Xu, 2014). So we compared the regional averaged diffusivity with flux from a local wind to inertial motions. We used 10 d averaged wind-induced near-inertial energy flux leading the observation of the CTD profile as the local wind flux. Like the variation of diffusivity, the wind flux was various every year, but a remarkable increasing trend could be identified in both regions (Figs 4 and 5). Yang and Wu (2012) find the energy transferred from wind to SCS has enhanced from 1959 to 2008. However, the variation of the spatial averaged diffusivities of flat and rough regions varied with depth (Fig. 6), this might contribute to the joint effort of the topography and the barotropic flow.

Comparing flat region with rough region, we can also find that topography play a considerable role for the turbulent diapycnal diffusivity (Figs 4 and 5). In the flat region, the maximum wind flux can nearly reach 0.8 mW/m^2, which was 50% larger than that in the rough region. However, comparing to diffusivity in the rough region, it was 30% to 50% less in the flat region. This resulted from the enhanced mixing around the topography (Tian et al., 2009; Wu et al., 2011; Jing and Wu, 2014). As shown in Fig. 4, with the propagating of the near-inertial wave, the energy can be dissipated by turbulence. While this process only appeared in the first two segments around the rough region (Figs 5 and 6). The diapycnal turbulence diffusivity decreased with depth in the flat region, contrasted with the rough region, where the diffusivity increased below 700 m. In flat region (Fig. 3), away from seabed (deeper than 2 600 m), the wind-stir played an important role in diapycnal mixing. However, in the rough region, the diapycnal mixing can be affected by both wind stress and internal tide. Even though the forth segment is away from seabed (more than 2 000 m, Fig. 6), the rapid change of topography in the east of selected rough region (Figs 2 and 3) may enhance the diapycnal mixing.

4 Summary and discussion

The fine-scale parameterization method was used to estimate the turbulent diapycnal diffusivity in the SCS along 18°N. We examined the influence of the wind-induced near-inertial energy flux and topographic roughness on diffusivity. It should be noted that, it was the first time discovering the enhanced turbulent diapycnal mixing trend resulting from the growth of the wind-induced near-inertial energy.

The temporal averaged diffusivity varied with depth. In the region far away from the bottom, the magnitude of the diapycnal diffusivity was 10^{-5} m^2/s, which was an order of magnitude less than the vertical-averaged diffusivity.

The enhanced turbulent diapycnal mixing trend had been found in the upper ocean at 18°N based on the CTD from 2005 to 2010, which resulted from the growth of energy from wind to near-inertial motions.

The total tidal dissipation rate is about 0.7–0.9 TW, which is one of the primary energy sources supporting diapycnal mixing, especially in the abyssal ocean (Munk and Wunsch, 1998). Tian et al. (2009) point out that the internal tide energy flux generated in the Luzon Strait supports diapycnal mixing and enhanced mixing in the SCS. This work also finds enhanced diapycnal mixing below 1 000 m near the Luzon Strait. However, the tidal dissipation rate may only contribute 50% of the energy required for mixing (Munk and Wunsch, 1998). Therefore, it has been argued that wind may supply a part of energy (Wunsch and Ferrari, 2004). Alford (2003) suggests that the total power from wind to near-inertial motions could can 0.47 TW. Jing et al. (2011) found a correlation between diapycnal diffusivity and wind stress on spatial-seasonal variations. The wind-induced near-inertial wave plays an important role on diapycnal mixing in the northwestern Pacific (Jing and Wu, 2014; Li and Xu, 2014), while there are seldom researches that study how it influence the SCS. In this work,

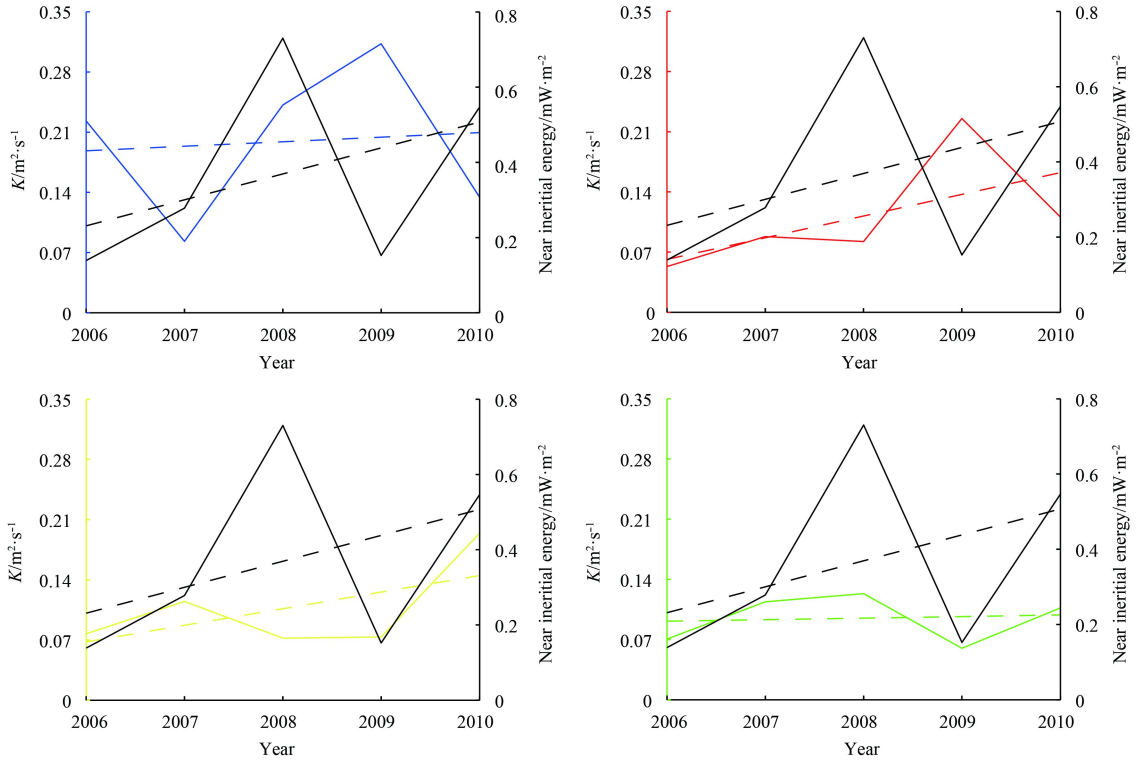

Fig. 4. Spatial (flat bathymetry) averaged diffusivity (colorful line) and wind-induced near-inertial flux (black solid line), which magnified 10^4 times for diffusivity. The dash line is trend for each variables. Blue for 256–512 m, red for 513–768 m, yellow for 769–1 024 m and green for 1 025–1 208 m.

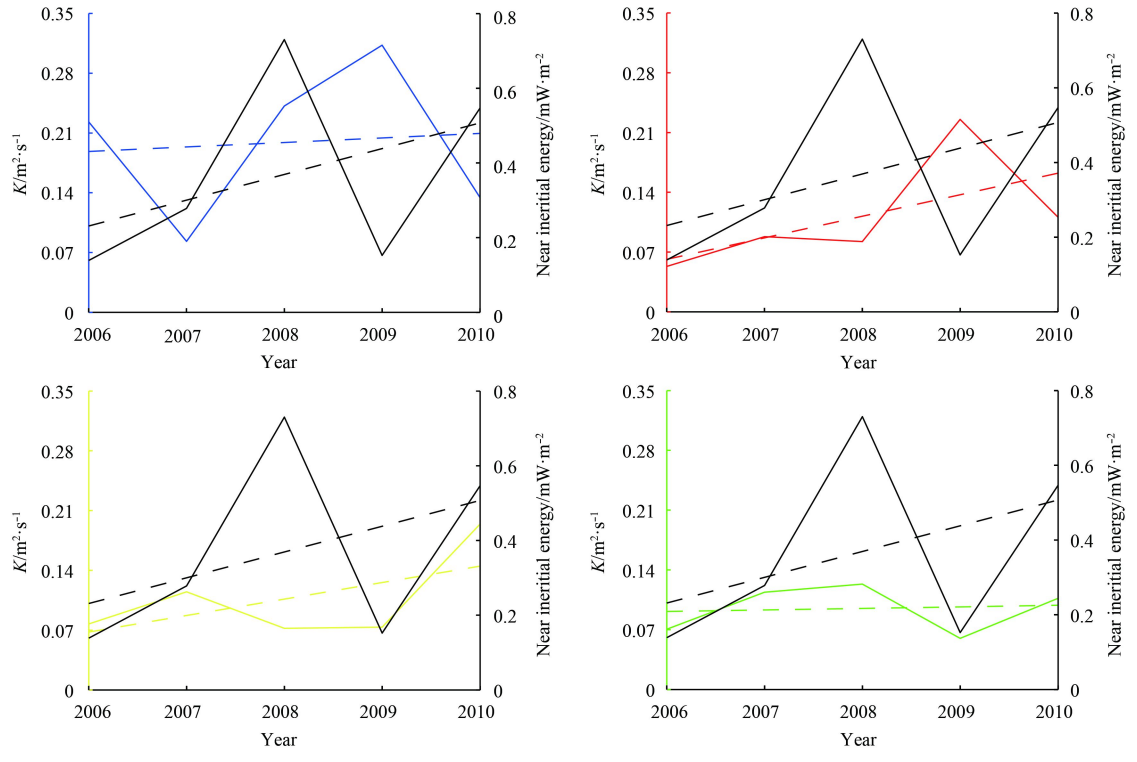

Fig. 5. Spatial (rough bathymetry) averaged diffusivity (colorful line) and wind-induced near-inertial flux (black solid line), which magnified 10^4 times for diffusivity. The dash line is trend for each variables. Blue for 256–512 m, red for 513–768 m, yellow for 769–1 024 m and green for 1 025–1 208 m.

we find the wind-induced near-inertial energy can enhance diapycnal mixing specially in the flat region where the internal energy flux is much weaker (Fig. 4), and the diffusivity decreases with the increase of depth (Fig. 6). It is different in the rough re-

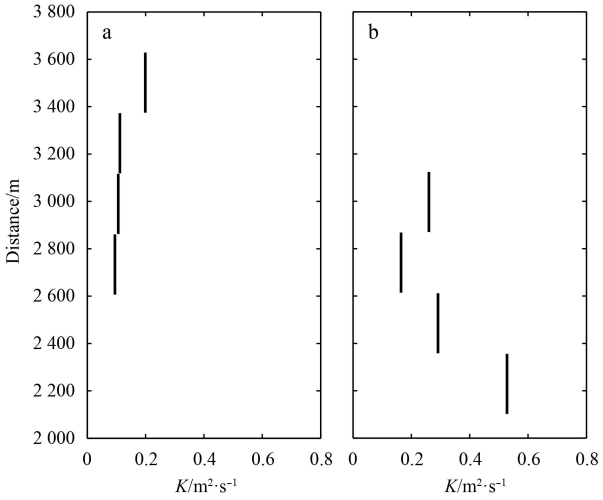

Fig. 6. The spatial averaged diffusivity of the upper four segments, which magnified 10^4 times, of flat (a) and rough (b) bathymetries varies with the distance from the seabed.

gion that the diffusivity increases with depth below 700 m owing to the joint effort of the topography and the barotropic flow (Fig. 6). The signal of growth of the enhanced diapycnal mixing resulting from the wind-induced near-inertial energy can be found in the upper three segments. There is still an argument about the depth that near-inertial waves can influence. Zhai et al. (2009) pointed out nearly 70% of the energy from wind working on near-inertial motions is lost within the top 200 m. However, recent researches indicate that the wind-induced near-inertial wave can penetrate up to 1 000 m (Wu et al., 2011; Li and Xu, 2014). Our study here indicates the growth of wind can enhance the mixing with depth extending to more than 700 m.

Acknowledgements

The authors thank the Key Laboratory of Tropical Marine Environment Dynamics, the South China Sea Institute of Oceanology, Chinese Academy of Sciences for providing the CTD data. We are grateful for the suggestions from Yang Qingxuan.

References

Alford M. 2001. Internal swell generation: the spatial distribution of energy flux from the wind to mixed layer near-inertial motions. J Phys Oceanogr, 31(8): 2359–2368

Alford M H. 2003. Improved global maps and 54-year history of wind-work on ocean inertial motions. Geophys Res Lett, 30(8): 1424

Alford M H, Peacock T, MacKinnon J A, et al. 2015. The formation and fate of internal waves in the South China Sea. Nature, 521(7550): 65–69

Egbert G D, Ray R D. 2001. Estimates of M2 tidal energy dissipation from TOPEX/Poseidon altimeter data. J Geophys Res, 106(C10): 22475–22502

Ge Lili, Cheng Xuhua, Qi Yiquan, et al. 2012. Upper-layer geostrophic volume, heat and salt transports across 18°N in the South China Sea. J Trop Oceanogr (in Chinese), 31(1): 10–17

Gill A E, Green J S A, Simmons A J. 1974. Energy partition in the large-scale ocean circulation and the production of mid-ocean eddies. Deep-Sea Res: Oceanogr Abstr, 21(7): 499–528

Gregg M C. 1987. Diapycnal mixing in the thermocline: a review. J Geophys Res, 92(C5): 5249–5289

Gregg M C, Kunze E. 1991. Internal wave shear and strain in Santa Monica basin. J Geophys Res, 96(C9): 16709–16719

Gregg M C, Sanford T B, Winkel D P. 2003. Reduced mixing from the breaking of internal waves in equatorial ocean waters. Nature, 422(6931): 513–515

Jayne S R, St Laurent L C. 2001. Parameterizing tidal dissipation over rough topography. Geophys Res Lett, 28(5): 811–814

Jing Zhao, Wu Lixin. 2010. Seasonal variation of turbulent diapycnal mixing in the northwestern pacific stirred by wind stress. Geophys Res Lett, 37(23): L23604

Jing Zhao, Wu Lixin. 2014. Intensified diapycnal mixing in the midlatitude western boundary currents. Sci Rep, 4: 7412

Jing Zhao, Wu Lixin, Li Lei, et al. 2011. Turbulent diapycnal mixing in the subtropical northwestern pacific: spatial-seasonal variations and role of eddies. J Geophys Res, 116(C10): C10028

Kunze E, Firing E, Hummon J M, et al. 2006. Global abyssal mixing inferred from lowered ADCP shear and CTD strain profiles. J Phys Oceanogr, 36(8): 1553–1576

Kunze E, Kennelly M A, Sanford T B. 1992. The depth dependence of shear finestructure off Point Arena and near Pioneer Seamount. J Phys Oceanogr, 22(1): 29–41

Li Ying, Xu Yongsheng. 2014. Penetration depth of diapycnal mixing generated by wind stress and flow over topography in the northwestern pacific. J Geophys Res, 119(8): 5501–5514

Munk W, Wunsch C. 1998. Abyssal recipes: II. Energetics of tidal and wind mixing. Deep-Sea Res: I, 45(12): 1977–2010

Pollard R T, Millard Jr R C. 1970. Comparison between observed and simulated wind-generated inertial oscillations. Deep-Sea Res: Oceanogr Abstr, 17(4): 813–816

Polzin K L, Toole J M, Schmitt R W. 1995. Finescale parameterizations of turbulent dissipation. J Phys Oceanogr, 25(3): 306–328

Tian Jiwei, Yang Qingxuan, Zhao Wei. 2009. Enhanced diapycnal mixing in the South China Sea. J Phys Oceanogr, 39(12): 3191–3203

Waterhouse A F, Mackinnon J A, Nash J D, et al. 2014. Global patterns of diapycnal mixing from measurements of the turbulent dissipation rate. J Phys Oceanogr, 44(7): 1854–1872

Whalen C B, Talley L D, MacKinnon J A. 2012. Spatial and temporal variability of global ocean mixing inferred from Argo profiles. Geophys Res Lett, 39(18): L18612

Wu Lixin, Jing Zhao, Riser S, et al. 2011. Seasonal and spatial variations of Southern Ocean diapycnal mixing from Argo profiling floats. Nat Geosci, 4(6): 363–366

Wunsch C, Ferrari R. 2004. Vertical mixing, energy, and the general circulation of the oceans. Annu Rev Fluid Mech, 36(1): 281–314

Yang Haiyuan, Wu Lixin. 2012. Trends of upper-layer circulation in the South China Sea during 1959–2008. J Geophys Res, 117(C8): C08037

Zhai Xiaoming, Greatbatch R J, Eden C, et al. 2009. On the loss of wind-induced near-inertial energy to turbulent mixing in the upper ocean. J Phys Oceanogr, 39(11): 3040–3045